Published OnlineFirst December 14, 2017; DOI: 10.1158/2159-8290.CD-17-0535

RESEARCH ARTICLE

Expressed Gene Fusions as Frequent Drivers of Poor Outcomes in Hormone Receptor–Positive Breast Cancer

Karina J. Matissek[1,2], Maristela L. Onozato[3], Sheng Sun[1,2], Zongli Zheng[2,3,4], Andrew Schultz[1], Jesse Lee[3], Kristofer Patel[1], Piiha-Lotta Jerevall[2,3], Srinivas Vinod Saladi[1,2], Allison Macleay[3], Mehrad Tavallai[1,2], Tanja Badovinac-Crnjevic[5], Carlos Barrios[6], Nuran Beşe[7], Arlene Chan[8], Yanin Chavarri-Guerra[9], Marcio Debiasi[6], Elif Demirdögen[10], Ünal Egeli[10], Sahsuvar Gökgöz[10], Henry Gomez[11], Pedro Liedke[6], Ismet Tasdelen[10], Sahsine Tolunay[10], Gustavo Werutsky[6], Jessica St. Louis[1], Nora Horick[12], Dianne M. Finkelstein[2,12], Long Phi Le[2,3], Aditya Bardia[1,2], Paul E. Goss[1,2], Dennis C. Sgroi[2,3], A. John Iafrate[2,3], and Leif W. Ellisen[1,2]

ABSTRACT We sought to uncover genetic drivers of hormone receptor–positive (HR+) breast cancer, using a targeted next-generation sequencing approach for detecting expressed gene rearrangements without prior knowledge of the fusion partners. We identified intergenic fusions involving driver genes, including *PIK3CA, AKT3, RAF1*, and *ESR1*, in 14% (24/173) of unselected patients with advanced HR+ breast cancer. FISH confirmed the corresponding chromosomal rearrangements in both primary and metastatic tumors. Expression of novel kinase fusions in nontransformed cells deregulates phosphoprotein signaling, cell proliferation, and survival in three-dimensional culture, whereas expression in HR+ breast cancer models modulates estrogen-dependent growth and confers hormonal therapy resistance *in vitro* and *in vivo*. Strikingly, shorter overall survival was observed in patients with rearrangement-positive versus rearrangement-negative tumors. Correspondingly, fusions were uncommon (<5%) among 300 patients presenting with primary HR+ breast cancer. Collectively, our findings identify expressed gene fusions as frequent and potentially actionable drivers in HR+ breast cancer.

SIGNIFICANCE: By using a powerful clinical molecular diagnostic assay, we identified expressed intergenic fusions as frequent contributors to treatment resistance and poor survival in advanced HR+ breast cancer. The prevalence and biological and prognostic significance of these alterations suggests that their detection may alter clinical management and bring to light new therapeutic opportunities. *Cancer Discov; 8(3); 1–18. ©2017 AACR.*

See related commentary by Natrajan, et al,. p. 272.

[1]Massachusetts General Hospital Cancer Center, Boston, Massachusetts. [2]Harvard Medical School, Boston, Massachusetts. [3]Department of Pathology, Massachusetts General Hospital, Boston, Massachusetts. [4]Department of Medical Epidemiology and Biostatistics, Karolinska Institutet, Stockholm, Sweden. [5]University Hospital Zagreb, Zagreb, Croatia. [6]Latin America Cooperative Oncology Group (LACOG) and Pontificia Universidade Catolica do Rio Grande do Sul (PUCRS), Porto Alegre, Brazil. [7]Department of Radiation Oncology, Acibadem Breast Research Institute, Istanbul, Turkey. [8]Mount Hospital, Perth, Australia. [9]Instituto Nacional de Ciencias Medicas y Nutrición Salvador Zubiran, México City D.F., México. [10]Departments of Medical Biology, General Surgery, Pathology of Medical Faculty of Uludag University, Bursa, Turkey. [11] Instituto Nacional de Enfermedades Neoplasicas, Lima, Perú. [12]Biostatistics Center, Massachusetts General Hospital, Boston, Massachusetts.

Note: Supplementary data for this article are available at Cancer Discovery Online (http://cancerdiscovery.aacrjournals.org/).

K.J. Matissek, M.L. Onozato, and S. Sun contributed equally to this article.

Corresponding Author: Leif W. Ellisen, Massachusetts General Hospital Cancer Center, 185 Cambridge Street, CPZN-4204, Boston, MA 02114. Phone: 617-726-4315; Fax: 617-726-8623; E-mail: lellisen@mgh.harvard.edu

doi: 10.1158/2159-8290.CD-17-0535

©2017 American Association for Cancer Research.

Downloaded from cancerdiscovery.aacrjournals.org on March 27, 2021. © 2017 American Association for Cancer Research.

Published OnlineFirst December 14, 2017; DOI: 10.1158/2159-8290.CD-17-0535

INTRODUCTION

The majority of primary breast cancers express estrogen receptor (ER) and progesterone receptor (PR) and are responsive to therapies that target the estrogen response pathway. Thus, ER and PR are favorable prognostic determinants and actionable therapeutic targets (1, 2). Nevertheless, a substantial minority of women treated for primary hormone receptor–positive (HR^+) disease exhibit hormonal therapy resistance, evidenced by the eventual development of metastatic disease. The pathways that confer hormonal therapy resistance have been studied extensively, yet our understanding of them remains relatively limited. Most notable among these are growth factor signaling networks that converge on the PI3K and MAPK pathways. Somatic mutations affecting these pathways are hallmarks of HR^+ breast cancer but are found in only a subset of tumors, suggesting that additional, undetected genetic events contribute to this disease (3).

The most frequent genetic alterations in primary HR^+ breast cancer are mutation or amplification of the PI3K catalytic subunit gene *PIK3CA* (30%–40% of tumors), mutation of the *TP53* tumor suppressor (≤30% of tumors), and amplification of the EGF family receptor gene *ERBB2* (HER2; approximately 25% of tumors; ref. 3). These and other, lower prevalence mutations occur in overlapping subsets of tumors, and consequently many tumors lack recognizable drivers. The recent identification of mutations in *ESR1* (encoding ERα) almost exclusively in treatment-refractory metastatic disease has suggested that metastases may harbor an additional proportion of disease-relevant mutations (4, 5). But even taken together, the genetic findings from standard exome sequencing and copy-number analyses are likely to represent at best a limited and incomplete picture of relevant genetic events in these tumors.

A potential group of relevant genetic events likely to be overlooked by exome-restricted DNA sequencing and traditional gene copy-number assessment are genomic rearrangements. Although whole-genome sequencing (WGS) can in theory detect many of these events, the complexity and "signal-to-noise" ratio in such analyses poses challenges, and many such rearrangements are not expressed as RNA (6). As expected, transcriptome-based analyses have also revealed the presence of intergenic fusions in breast cancer specimens (7–11). Routine detection of these events remains a challenge, however, and consequently their overall prevalence and potential clinical significance remain essentially unknown.

We recently reported the development and validation of a methodology, anchored multiplex PCR (AMP), for rapid and efficient targeted gene rearrangement detection (12). Here, we apply AMP systematically to cohorts of

Downloaded from cancerdiscovery.aacrjournals.org on March 27, 2021. © 2017 American Association for Cancer Research.

Published OnlineFirst December 14, 2017; DOI: 10.1158/2159-8290.CD-17-0535

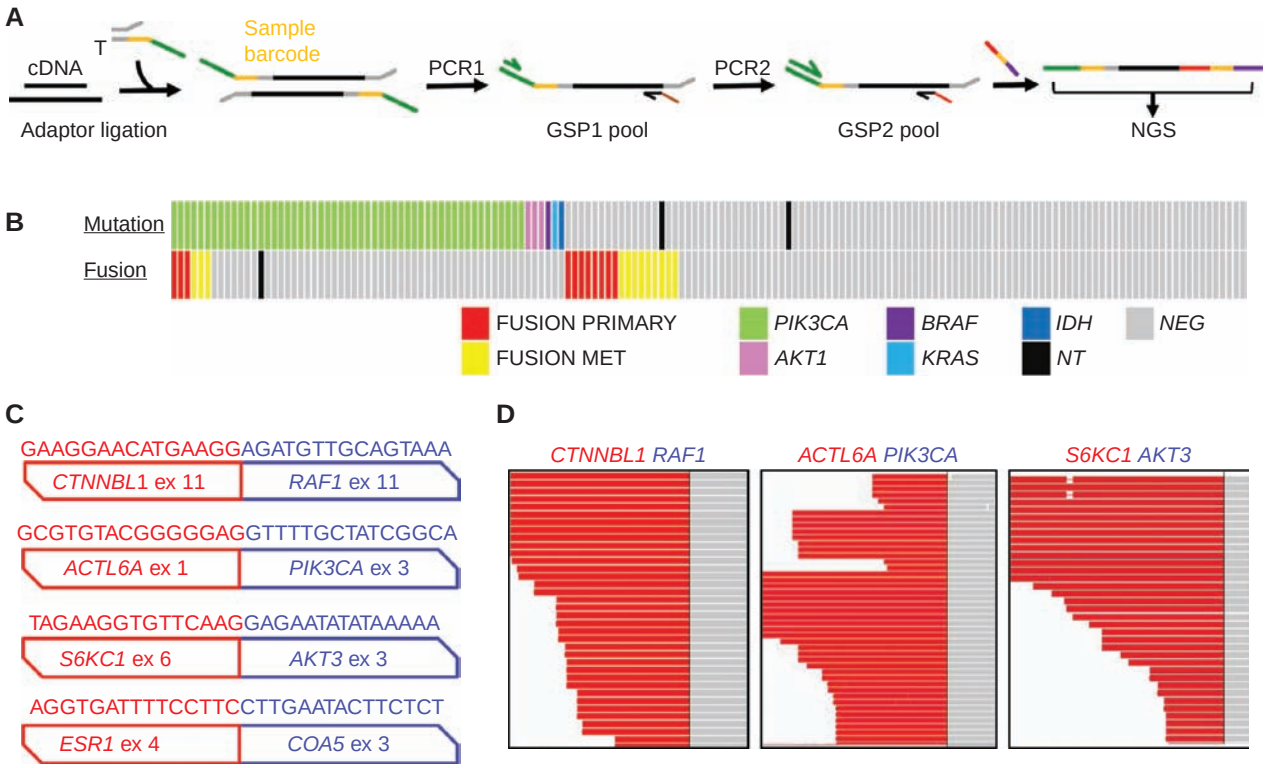

Figure 1. Expressed intergenic fusions are prevalent among patients with advanced HR+ breast cancer. **A,** Schematic flow diagram of AMP assay to detect expressed fusions, involving ligation to double-stranded cDNA of adaptor containing sample barcode, universal PCR priming site, and Illumina next-generation sequencing priming site, followed by two rounds of low-cycle PCR using one-sided, nested gene-specific primers (GSP) complementary to selected target exons. **B,** Summary of mutation and fusion detection among 173 patients with advanced HR+ breast cancer (Clinical Genotyping and Matched Primary/Metastasis Cohorts). Fusion Primary indicates detection in primary tumor ± metastatic tumor, whereas Fusion Met indicates detection only in the metastasis. NEG, none detected; NT, not tested. Tissue samples tested in a subset of cases were either primary tumors or metastatic lesions depending on availability (see text). Patients testing negative but not tested for both mutation and fusion assays are not shown. **C,** Representative identified fusions and their junction sequences involving the anchor genes *RAF1, PIK3CA, AKT3, ESR1*, and *BRAF*. Red, 5′ partner; blue, 3′ partner. **D,** Representative sequence read pileups from AMP analysis. The y-axis demonstrates read coverage; gray denotes anchor exon sequences and red shows the staggered distribution of reads with differing start positions in the nonanchored end of the sequence.

patients with early-stage and advanced HR+ breast cancers. Through complementary FISH analysis and functional studies, we reveal the frequent presence of novel, biologically and clinically relevant fusions involving potentially actionable genes and pathways in advanced HR+ breast cancer. The poor outcomes associated with these genetic lesions underscore the significance of our findings and the likely implications for breast cancer prognostication and treatment.

RESULTS

Prevalent Expressed Intergenic Fusions in Advanced HR+ Breast Cancer

AMP uses a mixture of tumor cDNA and genomic DNA as starting material. The assay has the major advantages that it does not require *a priori* knowledge of gene fusion partners and is compatible with low nucleic acid input from formalin-fixed, paraffin-embedded (FFPE) specimens (12). By using a nested, one-sided PCR approach AMP also allows identification of individual (pre-PCR) molecules, thereby mitigating PCR artifacts and facilitating quantitative gene expression analysis (Fig. 1A; ref. 12). We designed the AMP assay to detect fusions involving 54 solid tumor–relevant genes (Supplementary Table S1), and in our proof-of-concept study, we demonstrated a sensitivity of 100% and specificity of 100% compared with reference assays for gene rearrangement detection from FFPE samples (12).

We then applied AMP to tumor specimens from 110 sequential patients with advanced HR+ breast cancer who had presented to our clinic and had undergone clinical somatic tumor genotyping (Clinical Genotyping Cohort). This otherwise unselected patient cohort is representative of patients presenting with advanced HR+ disease, as most (>80%) had initially presented as stage II and higher, and the majority who presented with primary disease received adjuvant hormonal therapy (>90%) and/or chemotherapy (57%). Median age (49.5) was younger than average for such patients but is consistent with the demographic seen at an academic center (Supplementary Table S2). Remarkably, 14 of these patients harbored high-confidence intergenic fusions (Fig. 1B; Supplementary Table S3). Notably, the majority of these involved exon–exon fusions, including one case with an in-frame fusion of *ESR1* to *CCDC170*, which

Downloaded from cancerdiscovery.aacrjournals.org on March 27, 2021. © 2017 American Association for Cancer Research.

Published OnlineFirst December 14, 2017; DOI: 10.1158/2159-8290.CD-17-0535

has been previously reported to occur in <1% of HR+ breast cancers, and another with a fusion involving *BRAF* and the *SND1* gene, previously described in lung cancer (Supplementary Table S3; refs. 13, 14). The major identified fusion junction sequences in all cases involved at least one precise exon boundary, thereby defining the detected sequences as processed cDNA (Fig. 1C and D).

Because we wished to determine how often these fusions were present in primary tumors and the initial cohort represented a mix of primary and metastatic specimens, we next analyzed a second cohort of patients with advanced HR+ breast cancer ($N = 63$) for which both primary and matched metastatic specimens were available (Matched Primary/Metastasis Cohort; see Methods for cohort enrollment details). The clinical features of this patient cohort are very similar to those of the Clinical Genotyping Cohort, other than a slightly higher median age (58.5) and increased use of tamoxifen versus aromatase inhibitors in the adjuvant setting (Supplementary Table S2). The latter was expected, as a subset of these patients were enrolled at international sites where, until very recently, tamoxifen remained the most prescribed hormonal therapy agent. In this cohort, 10 of 63 patients were found to harbor a fusion in either the primary or metastatic specimen, 5 of which were detectable in the primary tumor (Supplementary Fig. S1A). Collectively, fusions were detected in 24 of 173 patients (14%), including 11 primary tumors (summarized in Fig. 1B). Notably, fully one-third of these fusions (8/24) involved *ESR1*, and multiple additional recurrent fusion targets were found in these cohorts, including two fusions each involving *AKT3, NOTCH1, PRKCA* (encoding protein kinase C), and *BRAF* (Supplementary Table S3). Among the most notable alterations identified were in-frame fusions involving the key oncogenic drivers *PIK3CA, AKT3, RAF1* (also known as *CRAF*), and *ESR1*, in each case fused to a distinct partner gene (Fig. 1C and D; Supplementary Fig. S1B and C).

In order to characterize these samples in more detail, we also performed mutational analysis using a site-specific, clinical laboratory assay that detects 120 recurrent mutations in 16 key cancer genes (Supplementary Table S4; ref. 15). We identified somatic driver mutations in 34% (59/173) of these patients, the majority involving *PIK3CA* as anticipated (Fig. 1B). Discordance between mutations detected in matched primary and metastatic specimens was noted as previously reported (16), and such discordance was also observed for fusions (Supplementary Fig. S1A). Interestingly, we did not observe a statistical association between the presence or absence of mutations and that of fusions in these cohorts (Fig. 1B).

In Situ Hybridization Confirms Fusion-Associated Genomic Rearrangements

As a next step to credential the potential relevance of these fusions, we sought to confirm the presence of the corresponding chromosomal rearrangements using an independent methodology, FISH. Approximately half of the detected intergenic fusions we identified involved genes on different chromosomes (Supplementary Fig. S2A). And among those involving genes on the same chromosome, in most cases the direction of transcription and/or centromere–telomere orientation predicted a genomic rearrangement detectable by FISH. We used a "break-apart" FISH strategy, incorporating different color probes 5′ and 3′ of the interrogated genetic loci, so that genomic rearrangement is evidenced by a separation of the normally juxtaposed red and green signals (Fig. 2A; ref. 17). The FISH approach also allowed us to ask whether these rearrangements were clonal (appearing in most or all identifiable tumor cells within a specimen), and whether they were present in primary tumors and metastases from the same patient.

FISH analysis confirmed a rearrangement of the respective locus in each AMP-positive tissue tested. Thus, FISH "break-apart" of the *RAF1* gene was evident in two distinct metastatic specimens from a patient harboring a *CTNNBL1–RAF1* fusion detected by AMP (Fig. 2B). Break-apart of *AKT3* was evident in both the primary and two metastatic specimens from a patient harboring an *RPS6KC1–AKT3* fusion detected by AMP (Fig. 2C). Notably, in this case, FISH identified both rearrangement and high-level amplification of the *AKT3* locus in the primary and metastatic lesions (Fig. 2C). Break-apart of *ESR1* was evident in a primary tumor and multiple metastases from a patient whose tumors all demonstrated an *ESR1–COA5* fusion upon AMP analysis (Fig. 2D). Additionally, the previously described *ESR1–CCDC170* fusion detected by AMP was confirmed upon FISH analysis for *ESR1* (Supplementary Fig. S2B). Finally, a fusion involving *BRAF* and the *SND1* gene was detected by AMP and was validated by FISH in two independent patients (Fig. 2E; ref. 14). We then developed IHC assays for RAF1 and AKT3 and observed high-level protein expression of the respective driver genes both in primary and metastatic tumors expressing these fusions (Supplementary Fig. S2C and S2D). Notably, fusion-negative breast cancer cases show little or no expression of these proteins. Collectively, these findings support fusions detected by AMP as *bona fide*, expressed genomic aberrations.

Oncogenic Activation of Signaling, Proliferation, and Survival by Novel Kinase Fusions

Several novel kinase-associated fusions we identified juxtapose a fully intact catalytic domain of the respective kinase to the partner gene (Supplementary Fig. S1B). In order to assess the potential contribution of these fusion proteins, we first analyzed their effects in nontransformed mammary epithelial cells (MCF10A). We synthesized cDNAs encoding predicted fusions involving *PIK3CA, RAF1*, and *AKT3* and introduced them via lentiviral vectors, demonstrating stable expression of proteins of the predicted molecular weight in each case (Fig. 3A). Furthermore, expression of these altered kinases was sufficient to activate mTORC1 signaling in these cells. This was evidenced by increases in phosphorylation of downstream substrates, including p70 S6 kinase (S6K1) and its substrate ribosomal protein S6 (RPS6), which was most evident in the absence of serum (Fig. 3B).

To assess the phenotypic effects of pathway activation by these kinase fusions, we determined their effect on acinar growth in three-dimensional (3-D) basement membrane

Downloaded from cancerdiscovery.aacrjournals.org on March 27, 2021. © 2017 American Association for Cancer Research.

Published OnlineFirst December 14, 2017; DOI: 10.1158/2159-8290.CD-17-0535

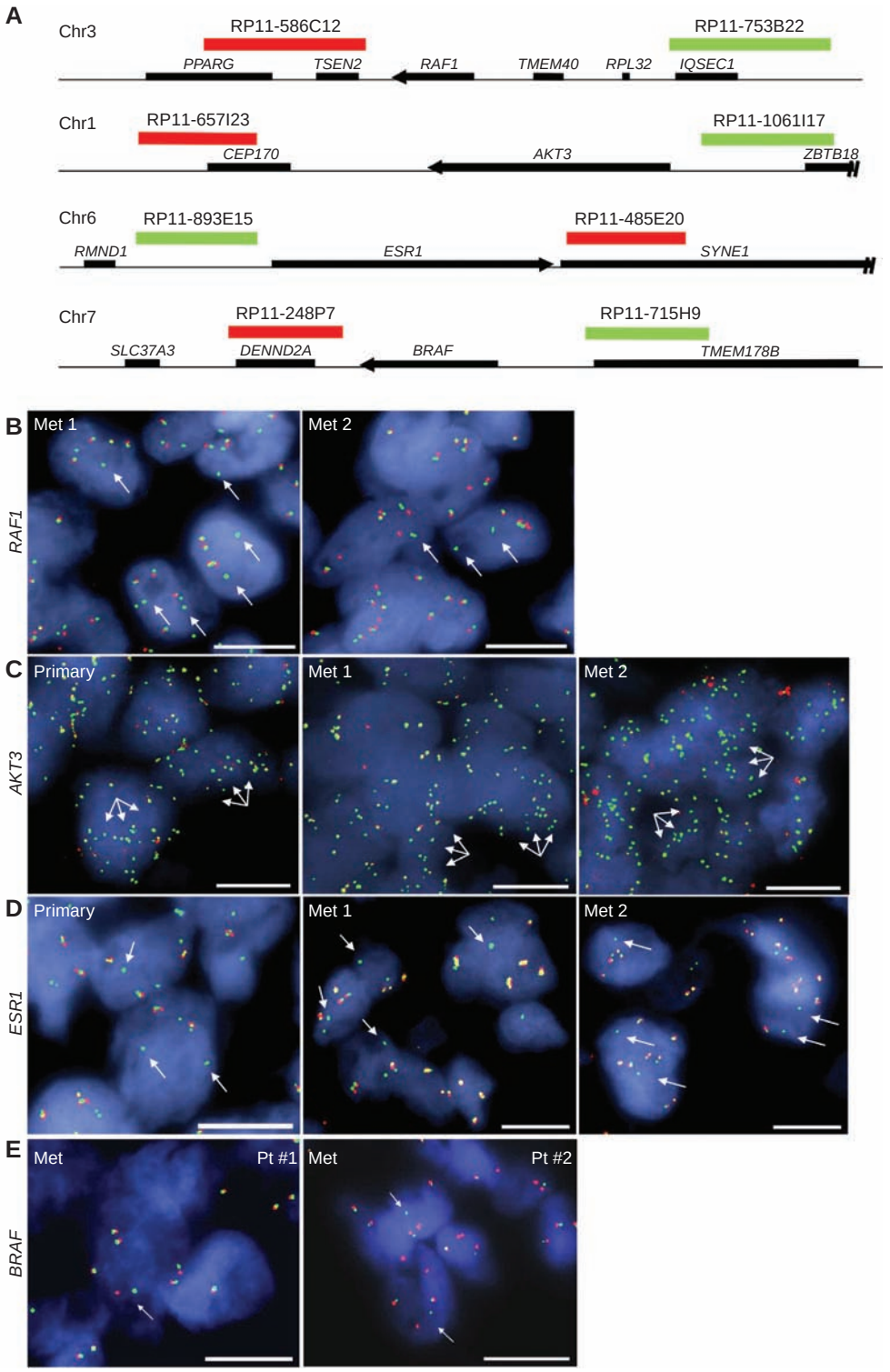

Figure 2. FISH analysis confirms fusion-associated genomic rearrangements in primary and metastatic tumors. **A,** Schematic diagram showing the identification and chromosomal localization of 5′ (green) and 3′ (red) BAC clones that served as FISH probes for the respective genes (black arrows) interrogated in AMP. All diagrams are oriented with ascending chromosomal location left to right. Adjacent genes are also shown (thick bars). **B–E,** Photomicrographs showing gene-specific rearrangement confirmation by FISH analysis of primary and patient-matched metastatic (Met) AMP+ tumors using red and green probes flanking the indicated genes. Adjacent red/green signals indicate an intact locus. White arrows indicate rearrangement (nonadjacent green or red signals). Rearranged *AKT3* locus also shows genomic amplification. The respective AMP-detected fusions are *CTNNBL1–RAF1*, *RPS6KC1–AKT3*, *ESR1–COA5*, and *BRAF–SND1*. A minimum of 200 nuclei were counted per specimen. Scale bars, 10 μm. (Note, *ACLT6A* and *PIK3CA* are adjacent genes not amenable to break-apart FISH analysis.)

Downloaded from cancerdiscovery.aacrjournals.org on March 27, 2021. © 2017 American Association for Cancer Research.

Published OnlineFirst December 14, 2017; DOI: 10.1158/2159-8290.CD-17-0535

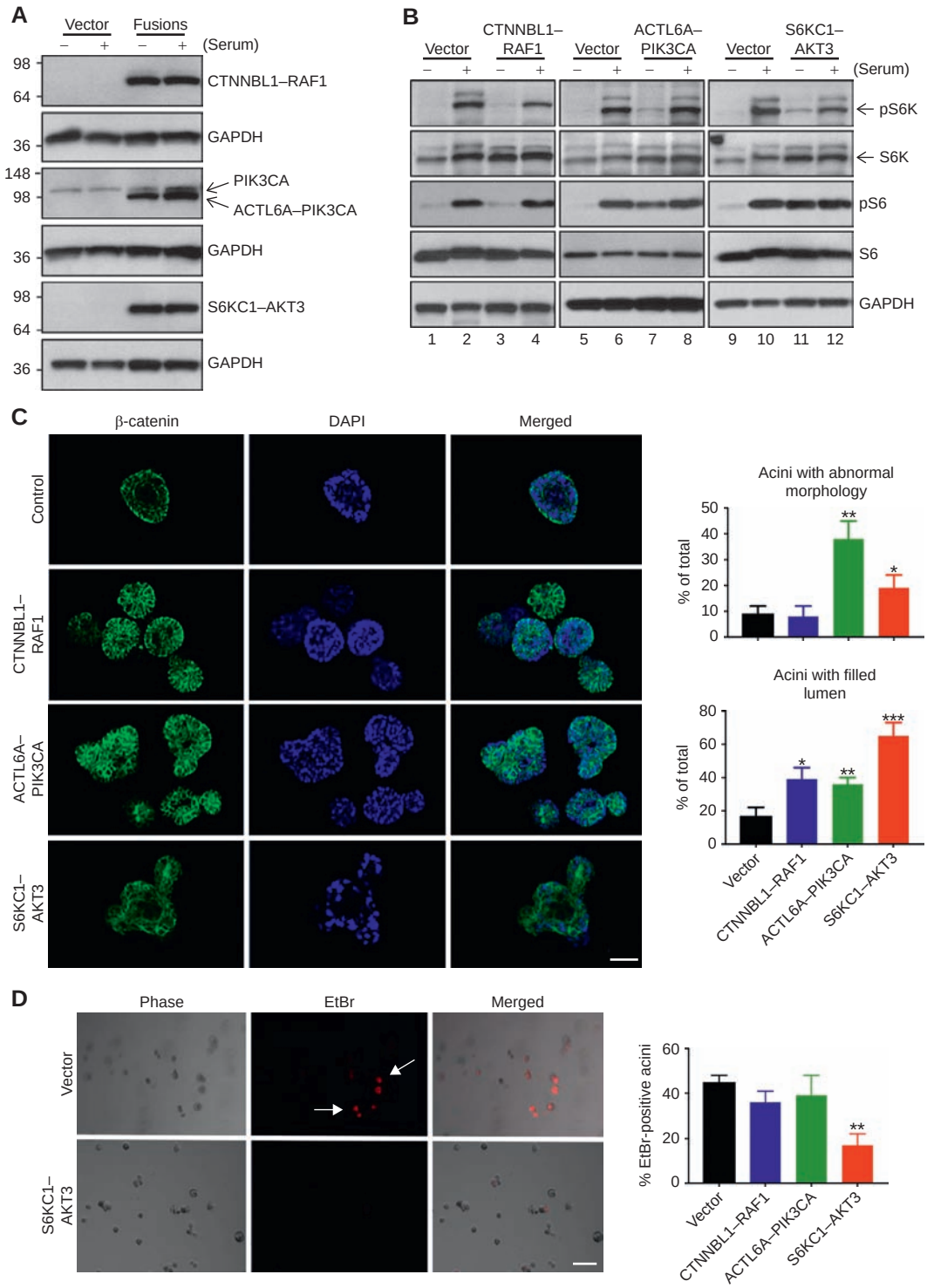

Figure 3. Novel kinase fusions promote oncogenic phenotypes in mammary epithelial cells. **A,** Western blot showing lentiviral-mediated expression of the indicated fusion proteins in MCF10A cells. Endogenous PIK3CA comigrates closely with ACLT6A–PIK3CA. **B,** Kinase fusions activate mTORC1 signaling, evidenced by increased pS6 kinase (pS6K, T389) and pS6 (S235/236) in Western analysis of lysates from MCF10A cells expressing the indicated fusions. Differences are most notable in the absence of serum. **C,** MCF10A cells were transduced with lentiviral vectors expressing the indicated fusions (left) followed by plating at clonal density in 3-D basement membrane culture. Scale bar, 50 μm. Right graphs show quantitation of deregulated growth and polarization (morphology) and cell survival (filled lumen) conferred by each fusion. Values plotted represent mean from eight replicate wells with 200 acini counted in each of three independent experiments. Error bars indicate SD. *P* values are determined by comparison in each case with vector using a two-tailed Student *t* test. *, $P < 0.05$; **, $P < 0.01$; ***, $P < 0.001$. **D,** AKT3 fusion promotes cell survival in 3-D culture. Left, photomicrographs of acini in Matrigel cultures stained with ethidium bromide (EtBr) to indicate cell death. Scale bar, 100 μm. Right, summary of EtBr-positive acini, counted and analyzed as described in **C**. **, $P < 0.01$.

Downloaded from cancerdiscovery.aacrjournals.org on March 27, 2021. © 2017 American Association for Cancer Research.

Published OnlineFirst December 14, 2017; DOI: 10.1158/2159-8290.CD-17-0535

(Matrigel) culture. Parental MCF10A cells produce stereotypical hollow spheres (acini) comprised of polarized cells in this setting, and deregulation of acinar morphology following introduction of various genes is known to correlate strongly with oncogenic properties of the respective genes in human breast cancer (18, 19). We found that expression of each fusion induced significant abnormalities in 3-D culture, and, furthermore, each produced a distinct disruption of the typical acinar growth. The PIK3CA fusion showed the strongest effect on cell growth, acinar morphology, and polarization, evidenced by the appearance of large, disordered structures (Fig. 3C). In contrast, all three fusions were associated with a significant increase in filled acinar structures (Fig. 3C). The filled acinar phenotype indicates defective apoptosis, because a well-described apoptotic program is known to be required for acinar luminal clearance in this setting (20).

We next used an independent assay to detect the apoptosis program in this context by staining acini with ethidium bromide, which is nonpermeable to viable cells. We found, as predicted, that control 3-D acinar structures exhibited ethidium-stained nuclei, indicating cell death, commensurate with luminal hollowing (Fig. 3D). In contrast, structures expressing the AKT3 fusion demonstrated near-complete absence of ethidium-stained cells, which correlated with the highest proportion of filled acinar lumens (Fig. 3D). The RAF1 and PIK3CA fusions conferred a nonsignificant trend toward decreased ethidium staining in 3-D culture (Fig. 3D; Supplementary Fig. S3), consistent with their effects on acinar filling (Fig. 3C). Thus, these kinase fusions activate phosphoprotein signaling and induce oncogenic deregulation of cell growth, polarity, and survival in mammary epithelia.

RPS6KC1–AKT3 Is a Constitutively Membrane Associated and Activated Kinase

We then sought to uncover a specific mechanism of fusion-mediated kinase deregulation. We focused on the fusion involving *RPS6KC1* and *AKT3*, as the encoded protein had the strongest effect on cell survival in 3-D culture. *RPS6KC1* encodes a pseudokinase whose amino terminus contains a PX domain, an established phosphoinositide (PI) binding motif (Fig. 4A; ref. 21). *AKT3* encodes an established oncogene that is frequently subject to genomic amplification in gliomas and other tumors (22). The identified fusion juxtaposes the PX domain of RPS6KC1 to a nearly intact AKT3 protein. Importantly, PX domains typically bind a broader variety of PI species than does the pleckstrin homology (PH) domain of AKT3 (21). Thus, we hypothesized that the kinase fusion might be rendered constitutively active by virtue of membrane recruitment in the absence of PI3K activation and subsequent PIP3 generation (Fig. 4A). To test this hypothesis, we performed a direct biochemical and functional comparison of the RPS6KC1–AKT3 fusion to wild-type AKT3. Expression of RPS6KC1–AKT3 and AKT3 at comparable levels in MCF10A indeed revealed increased basal phosphorylation of the fusion in the absence of serum (Fig. 4B; Supplementary Fig. S4A). Correspondingly, we observed elevated phosphorylation of the direct AKT substrates FOXO3A and Tuberin (TSC2) and of the downstream substrate RPS6 following expression of the fusion compared with wild-type AKT3 (Fig. 4B; Supplementary Fig. S4B).

In order to test directly the prediction that RPS6KC1–AKT3 was constitutively membrane associated, we fractionated serum-starved or stimulated cells expressing the fusion or wild-type AKT3. We observed the expected weak membrane localization of wild-type AKT3 in starved cells, followed by marked membrane recruitment with serum stimulation. In contrast, the fusion protein was constitutively membrane localized in multiple cell types and demonstrated no further membrane recruitment upon serum stimulation (Fig. 4C; Supplementary Fig. S4C and S3D). Consistent with these findings, expression of RPS6KC1–AKT3 induced nuclear exclusion of FOXO3A, which is known to be induced by phosphorylation, in MCF10A (Fig. 4D). The effects of this novel kinase were further corroborated in 3-D membrane culture, as the expression of the fusion produced large, disordered acini with filled lumens, which appeared identical to those described previously following expression of a constitutively active (myristoylated) AKT (Fig. 3C; ref. 23). Thus, RPS6KC1–AKT3 fusion produces a constitutively membrane-associated and activated kinase with oncogenic properties.

Deregulation of Hormone Dependence and Drug Response by Kinase Fusions

We hypothesized that these novel fusions, as potential drivers of hormone-dependent breast cancers, would alter hormone dependence and the response to hormonal therapy in cell-based HR^+ breast cancer models (24, 25). We therefore expressed three novel kinase fusions involving RAF1, AKT3, and PIK3CA in estrogen-dependent MCF7 and T47D breast cancer cells (Fig. 5A; Supplementary Fig. S5A). Both RAF1 and AKT3 fusions substantially activated downstream phosphoprotein signaling in these cells (Fig. 5B). Further demonstrating the activity of these kinases in this context, expression of the AKT3 fusion conferred resistance to a small-molecule AKT inhibitor (MK-2206), whereas expression of the RAF1 fusion conferred resistance selectively to the clinical MEK1/2 inhibitor trametinib (Supplementary Fig. S5B; refs. 26, 27).

Altered signaling induced by the different fusions produced remarkably distinct effects on hormone-dependent proliferation. Although MCF7 and T47D cells normally undergo complete arrest in the absence of estrogen, expression of the AKT3 fusion consistently conferred estrogen-independent proliferation in both models (Fig. 5C; Supplementary Fig. S5C; refs. 24, 25). We further tested hormone independence conferred by the AKT3 fusion using a recently described MCF7 derivative, $MCF7^{PIK3CAWT}$, in which the endogenous *PIK3CA* mutation in the parental line has been corrected via somatic gene targeting (28). Like parental MCF7, this line is highly estrogen-dependent for proliferation. Additionally, we directly compared effects of the AKT3 fusion in $MCF7^{PIK3CAWT}$ to that of an established transforming breast cancer mutant oncogene, $AKT1^{E17K}$ (29). Both AKT proteins potently induced downstream PI3K/mTORC1 signaling in $MCF7^{PIK3CAWT}$ cells (Supplementary Fig. S5D). We also observed that both the AKT3 fusion and $AKT1^{E17K}$ were sufficient to drive estrogen-independent proliferation in $MCF7^{PIK3CAWT}$ (Fig. 5D). Numerous studies

Downloaded from cancerdiscovery.aacrjournals.org on March 27, 2021. © 2017 American Association for Cancer Research.

Published OnlineFirst December 14, 2017; DOI: 10.1158/2159-8290.CD-17-0535

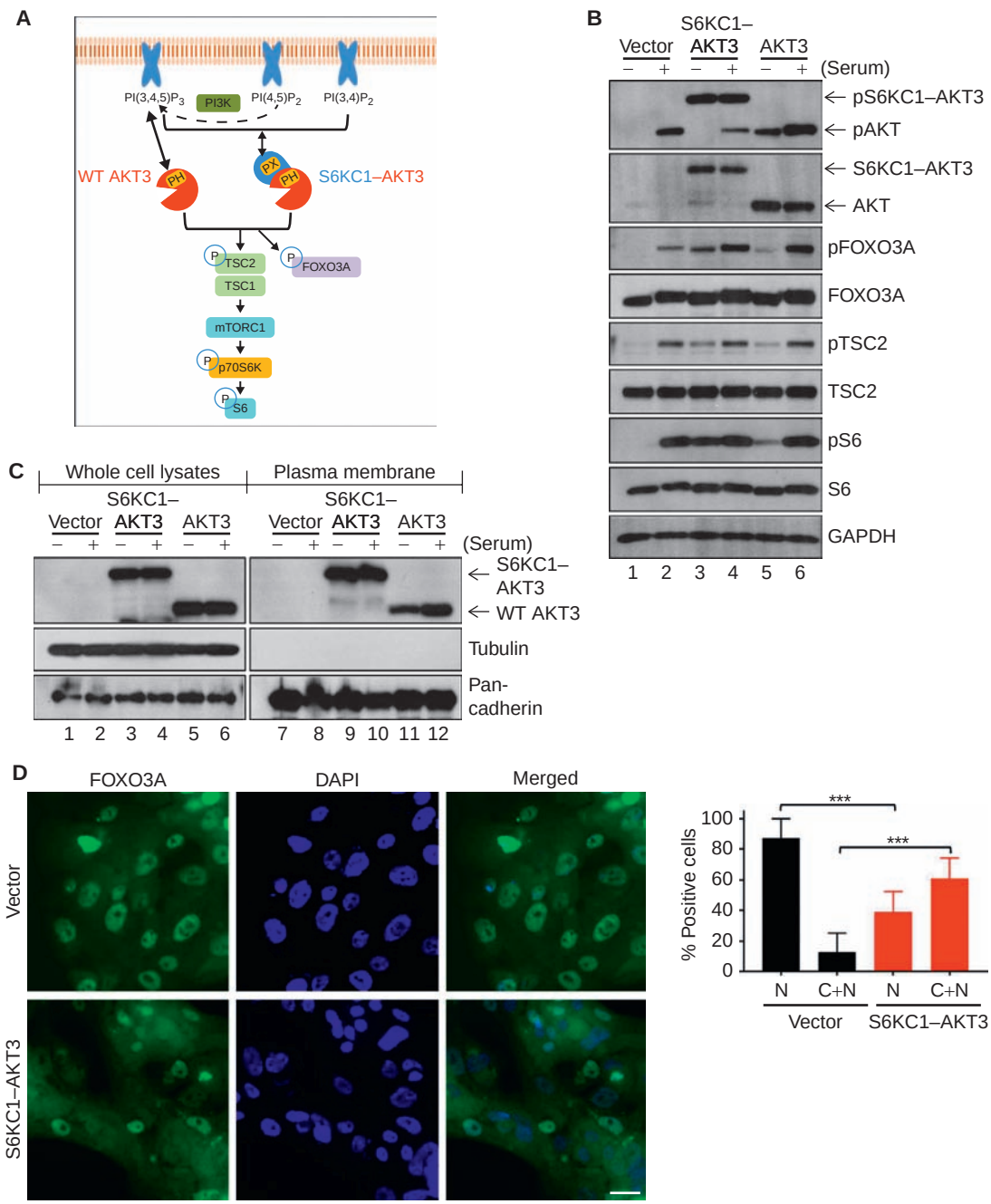

Figure 4. *RPS6KC1-AKT3* encodes a constitutively active kinase. **A,** Proposed model for fusion activation, mediated by constitutive association with diverse membrane phophoinositides via the RPS6KC1 PX domain, contrasting with AKT3, whose membrane-associated activation via the PH domain requires PI3K-dependent generation of PI(3,4,5)P_3. Downstream AKT substrates are also shown. **B,** Comparison of phosphoprotein signaling induced by ectopic AKT3 versus RPS6KC1-AKT3 fusion in MCF10A. In basal (serum-starved) condition, the fusion shows increased phosphorylation of itself (AKT S473), the direct AKT substrates FOXO3A (S253) and TSC2 (T1462), and downstream S6 (S235/236), compared with AKT3. **C,** RPS6KC1-AKT3 fusion is constitutively membrane localized in the absence of serum, shown in the plasma membrane fraction of MCF10A cells expressing the fusion or wild-type (WT) AKT3. (Compare lanes 9 vs. 10, 11 vs. 12.) Tubulin and pan-cadherin serve as controls for cytosol and membrane fractions, respectively. Summary data from multiple experiments for panels (**B**) and (**C**) are shown in Supplementary Fig. 4A–C. **D,** RPS6KC1-AKT3 expression is sufficient to induce nuclear export of FOXO3A, shown by immunofluorescence staining of MCF10A. At right, quantitation of nuclear (N) and cytosolic (C) FOXO3A staining, with 200 cells counted per condition in each of three independent experiments. *P* values by two-tailed Students *t* test. ***, $P < 0.001$. Scale bar, 50 μm.

Downloaded from cancerdiscovery.aacrjournals.org on March 27, 2021. © 2017 American Association for Cancer Research.

Published OnlineFirst December 14, 2017; DOI: 10.1158/2159-8290.CD-17-0535

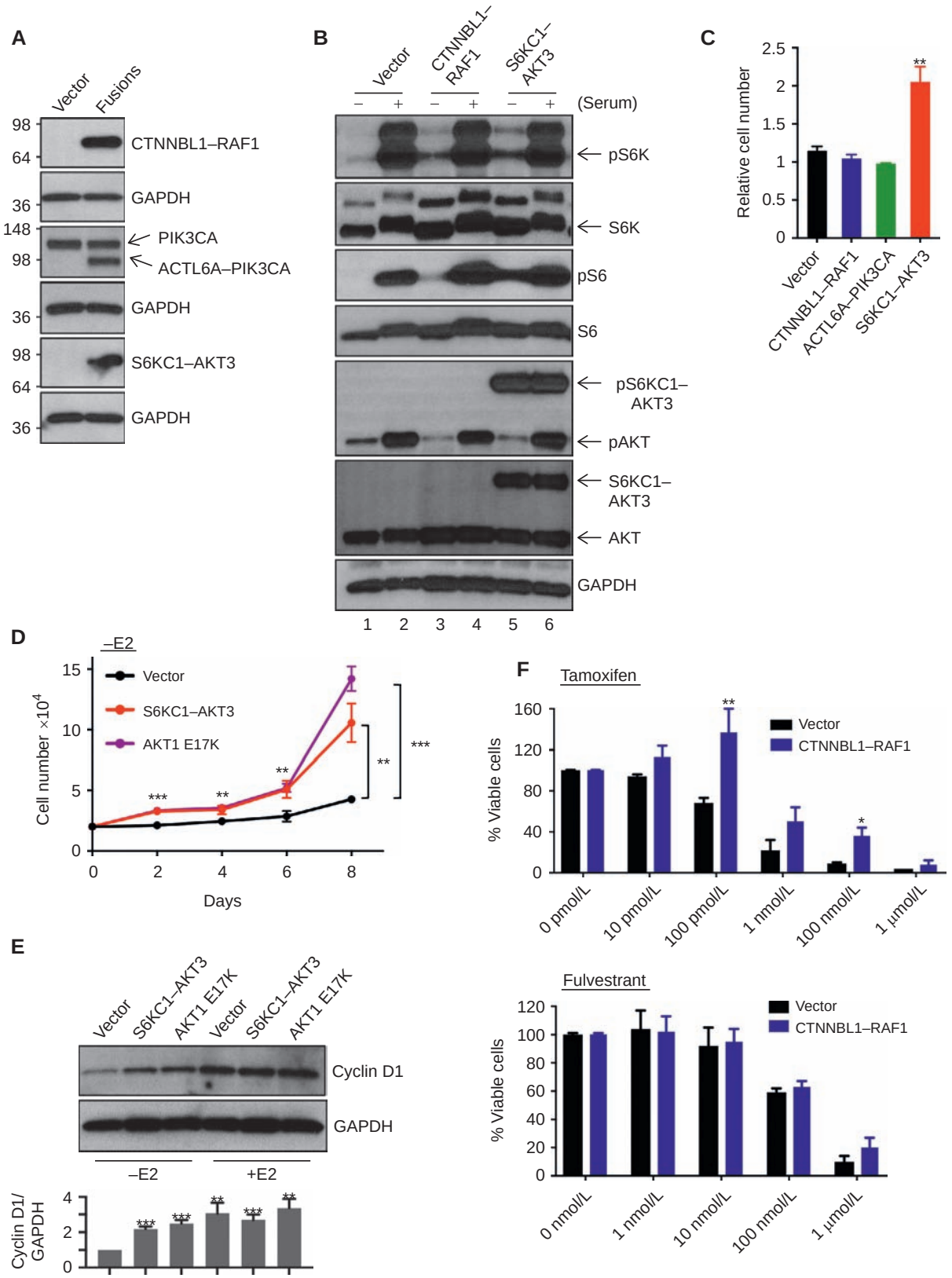

Downloaded from cancerdiscovery.aacrjournals.org on March 27, 2021. © 2017 American Association for Cancer Research.

Published OnlineFirst December 14, 2017; DOI: 10.1158/2159-8290.CD-17-0535

have linked such proliferation to AKT-dependent stabilization of cyclin D1 via phosphorylation of GSK3β (30). Accordingly, we observed that both the AKT3 fusion and AKT1^{E17K} expression triggered an increase in cyclin D1 levels in estrogen-starved MCF7^{PIK3CAWT} cells (Fig. 5E).

Distinct effects were observed with the RAF1 fusion, which did not confer estrogen-independent growth but instead switched the typical inhibitory effect of 4-OH tamoxifen, a competitive ER modulator, to a stimulatory one at low doses (Fig. 5F). In keeping with a receptor-dependent mechanism for this effect, the paradoxical stimulation was not observed with fulvestrant, which induces ER degradation (Fig. 5F). These findings are consistent with prior work showing that MAPK induces abnormal ER signaling that is opposed by pure estrogen antagonists but not by 4-OH tamoxifen (31). Receptor-dependent effects of each kinase fusion were further corroborated by analysis of the canonical ER transcriptional target genes *CCND1* (encoding cyclin D1) and *TFF1*. Cells expressing each kinase exhibited enhanced basal expression of these genes, whereas we observed distinct effects of the different fusions on estrogen-induced gene expression (Supplementary Fig. S5E).

RPS6KC1–AKT3 Drives Progression of Hormone-Dependent Tumors *In Vivo*

We next used an established *in vivo* model of HR+ breast cancer in order to further explore the potential oncogenic function of the AKT3 fusion (32). We transplanted T47D cells expressing either the RPS6KC1–AKT3 fusion or the control vector into the mammary fat pad of immunodeficient mice (Fig. 6A). As anticipated, control cells formed slow-growing tumors in the presence of exogenous estrogen (32). In contrast, fusion-expressing cells produced significantly larger tumors in less than one month (Fig. 6B). We then withdrew supplemental estrogen from these tumor-bearing mice, in order to mimic the effect of therapies such as aromatase inhibitors that function essentially by lowering systemic estrogen levels. As anticipated, control tumors were highly sensitive to estrogen deprivation, exhibiting significant regression in a period of days (Fig. 6C and D). Tumors expressing the AKT3 fusion, by comparison, showed no significant regression following estrogen withdrawal (Fig. 6C and D). We wished to compare these effects with those of a recognized transforming breast cancer gene and in the absence of a background *PIK3CA* mutation, so we repeated these experiments in MCF7^{PIK3CAWT}, transplanting cells expressing the AKT3 fusion, AKT1^{E17K}, or the control vector. Even controlling carefully for protein expression (Supplementary Fig. S5D), we observed a more highly significant increase in tumor progression with AKT3 fusion–expressing tumors than with AKT1^{E17K}-expressing tumors compared with the control vector (Supplementary Fig. S6A). Furthermore, upon estrogen withdrawal AKT3 fusion–expressing tumors showed minimal regression over a 2-week period. In contrast, vector-expressing MCF7^{PIK3CAWT} tumor regressed more than 30%, and AKT1^{E17K}-expressing tumors exhibited partial resistance (15% regression; Supplementary Fig. S6B and S6C).

A recent change to the standard approach for treatment of advanced HR+ breast cancer involves the combination of hormonal therapy with inhibitors of the cell-cycle regulatory cyclin-dependent kinases CDK4 and CDK6 (33). Accordingly, we tested whether the combination of estrogen withdrawal and the CDK4/6 inhibitor palbociclib could overcome therapeutic resistance conferred by AKT3 fusion expression *in vivo* (Fig. 6A). Remarkably, this combination completely abolished the advantage observed in fusion-expressing tumors, inducing a regression in both these and control tumors substantially more profound than that induced by hormone withdrawal alone (Fig. 6E). To corroborate these effects at the cellular level, we stained the resulting tumors for the proliferation marker Ki67, an established correlate of response in human breast cancer (34). Although AKT3 fusion–expressing tumors exhibited a marginally higher Ki67 fraction than control tumors following estrogen withdrawal, palbociclib treatment virtually eliminated Ki67-positive cells in both cases (Fig. 6F and G). Biochemical analysis further supported the ability of palbociclib to overcome effects of the activated AKT3 fusion. Phosphorylated retinoblastoma protein (RB1), the target of CDK4/6, was elevated in the absence of estrogen in AKT3 fusion–expressing cells compared with controls, but was completely suppressed in both cases following palbociclib treatment (Fig. 6H). Thus, this activated kinase fusion confers resistance to traditional hormonal therapy approaches that can be overcome by newly available therapeutic combinations.

Intergenic Fusions Are Enriched in Advanced Disease and Confer Decreased Overall Survival

Taken together, the findings above imply a contribution of identified fusions to aggressive behavior and treatment

Figure 5. Deregulation of hormone-dependent growth, transcription, and drug response mediated by novel kinase fusions. **A,** Lentiviral-mediated expression of the indicated kinase fusion proteins in MCF7 cells. **B,** Activation of mTORC1 signaling following kinase fusion expression in serum-starved MCF7 cells, evidenced by increased pS6 kinase (pS6K, T389) and pS6 (S235/236). Constitutive phosphorylation of RPS6KC1–AKT3 (AKT S473) is also apparent compared with endogenous AKT. **C,** RPS6KC1–AKT3 fusion expression confers estrogen-independent proliferation in MCF7 cells propagated in charcoal-stripped serum for 5 days. Values plotted show the number of cells at day 5 relative to day 0 and represent the mean of quadruplicate wells in a representative experiment performed 5 times. Error bars, SD. *P* value was determined by comparison in each case to vector using a two-tailed Student *t* test. **, $P < 0.01$. **D,** Estrogen-independent proliferation is conferred by RPS6KC1–AKT3 in MCF7^{PIK3CAWT} cells expressing the indicated lentiviral vectors, propagated in charcoal-stripped serum for 8 days. Proliferation is comparable to that induced by AKT1 E17K. Values plotted represent the mean of quadruplicate wells in a representative experiment performed 3 times. *P* value was determined by Student *t* test at each time point. **E,** RPS6KC1–AKT3 and AKT1 E17K expression promote comparable cyclin D1 expression under estrogen withdrawal in MCF7^{PIK3CAWT} cells. Cells were propagated in charcoal-stripped serum for 3 days (−E2), followed by estrogen pulse (+E2, 100 pmol/L, 12 hours) prior to harvest. Shown is a representative experiment performed three times. Bar graph below shows the mean result of three independent experiments, analyzed by densitometry for cyclin D1/GAPDH ratio. **F,** CTNNBL1–RAF1 expression induces paradoxical growth stimulation at 100 pmol/L of tamoxifen but not with fulvestrant treatment in MCF7 cells. Values plotted represent the mean of quadruplicate wells in a representative experiment performed 3 times. *P* value was determined by two-tailed Student *t* test at each dose. Except as indicated, dose-specific comparisons between vector and fusion are nonsignificant. *, $P < 0.05$; **, $P < 0.01$; ***, $P < 0.001$.

Downloaded from cancerdiscovery.aacrjournals.org on March 27, 2021. © 2017 American Association for Cancer Research.

Published OnlineFirst December 14, 2017; DOI: 10.1158/2159-8290.CD-17-0535

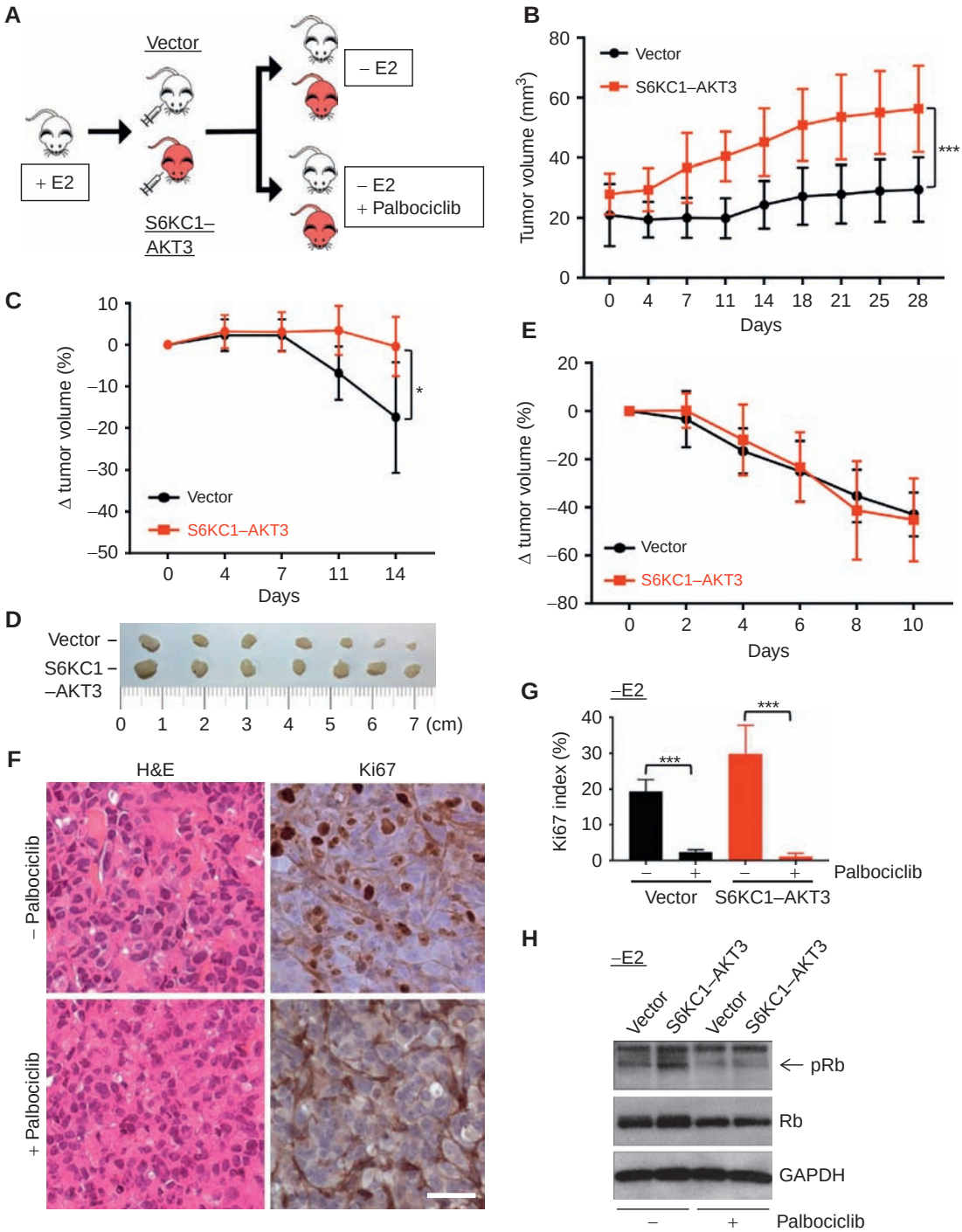

Figure 6. The RPS6KC1-AKT3 kinase fusion promotes tumor progression and confers hormonal therapy resistance *in vivo*. **A,** Schematic experimental outline. Tumors are established by injection of T47D cells expressing the control vector or RPS6KC1-AKT3 into mammary fat pads of mice bearing supplemental estrogen (E2) tablets. **B,** RPS6KC1-AKT3 promotes tumor growth *in vivo*. Vector, $N = 19$; RPS6KC1-AKT3, $N = 19$. Note that day 0 is defined as the first-day measurable tumors evident in both populations, 7 days after injection. *P* value was determined by two-way multiple-measures ANOVA. ***, $P < 0.001$. **C,** Tumor-bearing mice underwent supplemental estrogen withdrawal (day 0, 41 days after injection). Tumors expressing RPS6KC1-AKT3 ($N = 7$) fail to regress relative to control tumors ($N = 9$). *P* value determined as in **B**. **D,** The representative tumors from **C** at day 49. *, $P < 0.05$. **E,** Palbociclib (150 mg/kg/day) plus supplemental estrogen withdrawal (beginning day 0 as in **C**) induces tumor regression and overcomes resistance mediated by RPS6KC1-AKT3 to estrogen withdrawal alone. Vector, $N = 10$; RPS6KC1-AKT3, $N = 8$. **F,** Palbociclib abolishes cell cycling in RPS6KC1-AKT3-expressing tumors, evidenced by loss of Ki67 nuclear staining in representative histologic sections of tumors from **C** and **D**. Corresponding histologic staining is shown at left. H&E, hematoxylin and eosin. Scale bar, 50 μm. **G,** Quantitation of Ki67 staining in control and RPS6KC1-AKT3-expressing tumors from **C** and **D,** showing comparable reductions by palbociclib in both cases. Graph represents >20 high-powered fields counted per tumor for 4 tumors in each group. Error bars, SD. ***, $P < 0.001$. **H,** Phosphorylated RB1 (Rb, S780) is increased in estrogen-starved RPS6KC1-AKT3-expressing cells but is extinguished by palbociclib (500 nmol/L, 24 hours).

Downloaded from cancerdiscovery.aacrjournals.org on March 27, 2021. © 2017 American Association for Cancer Research.

Published OnlineFirst December 14, 2017; DOI: 10.1158/2159-8290.CD-17-0535

resistance in HR+ breast cancer. To test this possibility in patients we analyzed the impact of fusions on clinical outcomes. These included time from initial diagnosis to metastatic disease recurrence, survival from time of metastasis, and overall survival (35). To assess the potential for confounding in the association between fusion status and these outcomes, we conducted a stratified analysis comparing the distribution of clinical characteristics between fusion-positive and fusion-negative groups, controlling for the effect of cohort (Clinical Genotyping and Matched Primary/Metastasis Cohorts). Clinical characteristics did not differ significantly by fusion status, suggesting that any association between fusion status and survival would not be affected by clinical confounders (Supplementary Table S2).

Kaplan–Meier curves were then constructed to illustrate the relationship between fusion or mutation status and each clinical outcome. Cox proportional hazards models, stratified by cohort, were used to assess the association between clinical outcomes, fusions, and mutations. (Notably, as these cohorts represented patients treated prior to 2015, no patients received CDK4/6 inhibitors as either adjuvant therapy or early-line treatment in the metastatic setting.) Patients with fusion-positive tumors demonstrated a trend toward shorter time from initial diagnosis to metastatic recurrence (TTR) than those with fusion-negative tumors [Fig. 7A, hazard ratio (HR) = 1.56, $P = 0.06$]. By comparison, the subset of somatic oncogenic driver mutations assessed in these cohorts were not associated with differences in TTR (Fig. 7B, HR = 1.04,

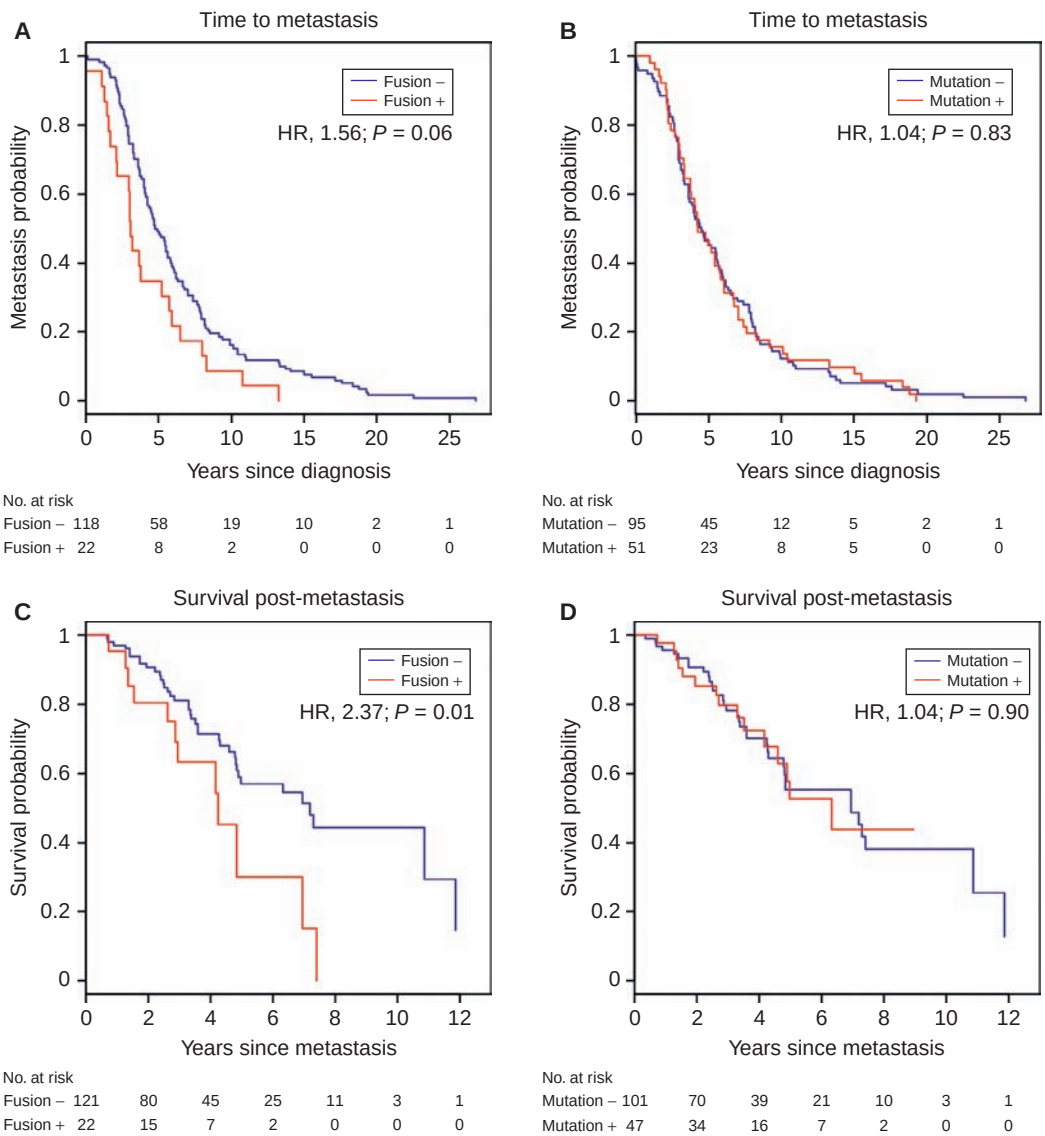

Figure 7. Expressed intergenic fusions are associated with an aggressive clinical course and short survival. **A** and **B,** Kaplan–Meier analysis demonstrating a trend toward shorter time to metastasis for patients whose tumors were positive versus negative for (**A**) gene fusion [hazard ratio (HR) = 1.56; $P = 0.06$] but not for (**B**) assessed somatic mutations (HR = 1.04; $P = 0.83$). **C** and **D,** Shorter survival time post development of metastasis for (**C**) fusion-positive versus fusion-negative patients (HR = 2.37; $P = 0.01$) but not for (**D**) mutation-positive versus mutation-negative patients (HR = 1.04; $P = 0.90$). (*continued on next page*)

Downloaded from cancerdiscovery.aacrjournals.org on March 27, 2021. © 2017 American Association for Cancer Research.

Published OnlineFirst December 14, 2017; DOI: 10.1158/2159-8290.CD-17-0535

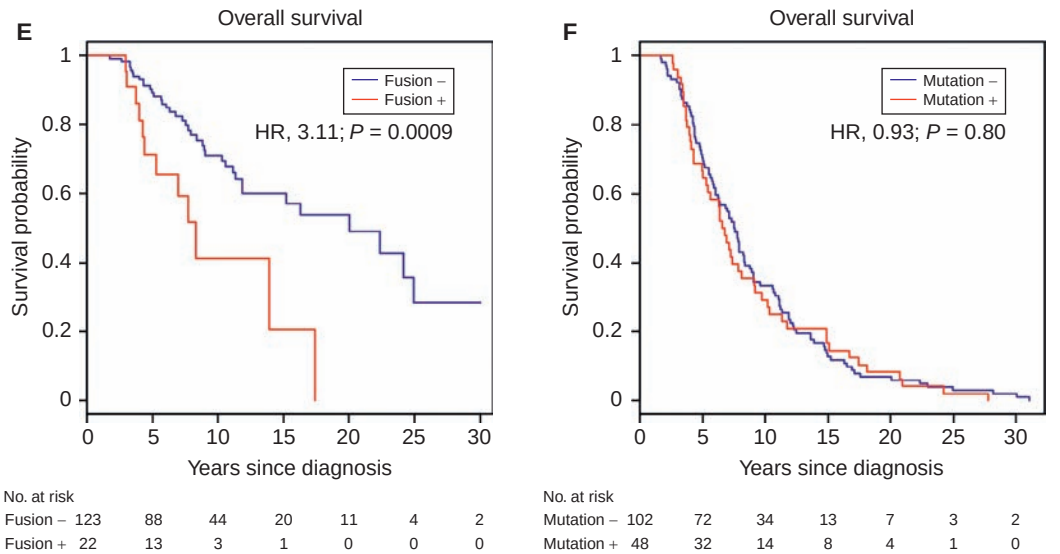

Figure 7. ***(Continued)*** **E** and **F,** Shorter overall survival from time of initial breast cancer diagnosis for (**E**) fusion-positive versus fusion-negative patients (HR = 3.11; $P = 0.0009$) but not for (**F**) mutation-positive versus mutation-negative patients (HR = 0.93; $P = 0.80$). Cox proportional hazards models were used in each case to assess the association between clinical outcomes and fusions and mutations. Numbers of patients with available data for each analysis are indicated, as described in Methods. Clinical characteristics did not differ significantly between fusion-positive and fusion-negative patients (Supplementary Table S2).

$P = 0.83$). Most strikingly, fusion-positive status was associated with highly significant decreases both in survival from time of metastatic recurrence (Fig. 7C, HR = 2.37, $P = 0.01$) and in overall survival (OS) from time of initial diagnosis (Fig. 7E, HR = 3.11, $P = 0.0009$). In contrast, the assessed somatic mutations were not significantly associated with either of these survival metrics (Fig. 7D and F).

Finally, we tested the hypothesis that as drivers of poor outcomes, fusions would be less common among patients presenting with primary (nonmetastatic) HR$^+$ breast cancer, the large majority of whom are cured. Thus, we assembled a cohort of 300 such patients (Primary Diagnosis Cohort; Supplementary Table S5) and created tissue microarrays of the primary tumors, allowing us to screen the entire cohort by FISH for fusions corresponding to the most commonly implicated fusion genes. Analysis of all cases with probes for *PIK3CA, ESR1, RAF1,* and *AKT3* (which together comprised approximately half of the fusions among our cohorts with advanced HR$^+$ cancer) revealed only 12 possibly abnormal patterns by FISH. Furthermore, subsequent molecular analysis of these cases with the AMP assay demonstrated only a single *bona fide* fusion involving *ESR1* and *CCDC170* (Supplementary Table S6). Although this was not a complete analysis of all possible fusions and was by design limited to analysis of primary tumors, these results are consistent with a high prevalence of fusions selectively in patients with biologically aggressive metastatic disease and poor outcomes.

DISCUSSION

This study reveals the remarkable prevalence of expressed intergenic fusions involving key cancer genes in patients with advanced HR$^+$ breast cancer. The direct contribution of these genomic alterations to the pathophysiology of these cancers is supported by a number of our observations. First, we confirmed by FISH that these genomic rearrangements are present within the tumor and are associated with protein expression. Second, we observed that the rearrangements and protein expression can be found in both primary and/or multiple matched metastases from the same patient. Third, we provide evidence that multiple novel fusions produce active and deregulated kinases that confer oncogenic phenotypes in breast epithelial models. Fourth, we demonstrate that such fusions are sufficient to disrupt hormonal-dependent proliferation, transcription, and tumor progression in HR$^+$ breast cancer models both *in vitro* and *in vivo*. Notably, the most prevalent fusions detected involve *ESR1*, a finding that supports their relevance to the pathogenesis of HR$^+$ breast cancer. Finally, we show that patients whose tumors harbor these fusions have markedly more rapid progression and shorter survival than fusion-negative patients.

Our analyses also reveal that these gene fusions appear distinct in their implications from other common somatic genetic events in HR$^+$ breast cancer. For example, somatic mutations in *PIK3CA* are common in tumors of patients presenting with primary (curable) disease, and in this setting are generally associated with more favorable outcomes (36). In contrast, somatic mutations in *ESR1* are found almost exclusively in metastatic lesions, and typically only in the setting of acquired resistance to multiple prior rounds of hormonal therapy (4, 5). The fusions we have uncovered are present in some cases in both primary and metastatic tumors, whereas in other cases only in metastases, and prior to specific therapy in the metastatic setting. Their enrichment selectively in patients who develop metastatic disease is consistent with a role in *de novo* treatment resistance, whereas their appearance

Downloaded from cancerdiscovery.aacrjournals.org on March 27, 2021. © 2017 American Association for Cancer Research.

Published OnlineFirst December 14, 2017; DOI: 10.1158/2159-8290.CD-17-0535

in metastases could in those cases reflect a contribution to acquired resistance.

Our findings are in keeping with the emerging concept of gene fusions as frequent oncogenic drivers in many solid tumors (11). Until recently, however, the prevalence of these genetic events has been largely overlooked because most clinical tumor genotyping analyses (e.g., exome sequencing) do not analyze RNA and therefore fail to detect such fusions. Nonetheless, a growing body of evidence demonstrates that these species, and particularly activated kinase fusions, may represent viable therapeutic targets in multiple cancers (37). The expanding therapeutic arsenal of kinase pathway inhibitors further implies that such fusions, as well as ER gene fusions, may be immediately actionable in the setting of appropriately designed clinical trials (38). An individualized approach to targeting these fusions will likely be required, however, as evidenced by the distinct effects of different fusions on hormonal signaling and cell growth that we observe.

Despite their heterogeneity, our detailed analysis of the AKT3 fusion suggests that newly approved therapies for HR+ breast cancer including CDK4/6 inhibitors may overcome treatment resistance associated with some fusions. As noted, patients in this study did not receive CDK4/6 inhibitors as treatment for their primary disease, as these agents are not yet FDA approved for this indication. However, two additional patients harboring fusions we subsequently identified who developed metastatic HR+ disease following standard hormonal therapy did receive a combination of hormonal therapy and a CDK4/6 inhibitor for treatment of their metastatic disease. Both of these patients experienced significant clinical benefit. Because our study implies that patients with fusion-positive tumors are more likely to develop metastatic disease, the potential ability of CDK4/6 inhibitors to overcome fusion-mediated hormonal therapy resistance could portend a positive impact on relapse-free survival in the adjuvant treatment of early-stage breast cancer, an indication for which clinical trials are currently ongoing (39).

In summary, our findings reveal intergenic fusions as frequent drivers of treatment resistance and poor outcomes in advanced HR+ breast cancer. Given their presence in primary tumors and their association with poor survival that we demonstrate, it seems likely that routine detection of such alterations could ultimately lead to successful targeting and a major impact on long-term disease outcomes.

METHODS

Tissue Samples and Clinical Data Collection

The Clinical Genotyping Cohort comprised a retrospective set of sequential patients with advanced ER+ and/or PR+ breast cancer who presented to Mass General and underwent local somatic genotyping by physician order between 2010 and 2014. All were tested for HER2 by IHC and/or FISH and none were positive. A single tissue sample was tested by AMP (either primary tumors or metastatic lesions depending on availability). The only exclusion was for nucleic acid samples that did not pass QC analysis for AMP testing. The Primary Diagnosis Cohort comprised a retrospective set of patients with who presented with primary ER+ and/or PR+ breast cancer and had locally available FFPE primary tumor tissue. For these two cohorts, retrospective use of discarded, clinically collected tissue, and limited clinical data was reviewed and approved by the Mass General/Harvard Cancer Center (HCC) Institutional Review Board (IRB) with waiver of consent. The Matched Primary/Metastatic Cohort included patients with available matched tissue specimens who presented with advanced ER+ and/or PR+ breast cancer to collaborating international institutions or Mass General between 2000 and 2012. All except four underwent HER2 testing by IHC and/or FISH; five were positive (all fusion-negative) and none received anti-HER2 therapy. Eligible patients signed written informed consent for participation in the study, which was approved by the HCC IRB and the individual local IRBs, all of which follow the U.S. Common Rule or the International Ethical Guidelines for Biomedical Research Involving Human Subjects (CIOMS). Concordance between fusion detection in primary and metastatic tumors for this cohort is illustrated in Supplementary Fig. S1A.

DNA Extraction, Anchored Multiplex PCR, and Somatic Genotyping

The methodology for each of these has been described previously (12, 15). Briefly, total nucleic acids containing total RNA and genomic DNA were extracted from FFPE tissue specimens, using the Agencourt FormaPure Kit for FFPE Tissue (Beckman Coulter). For AMP analysis, first- and second-strand complementary DNA (cDNA) synthesis was performed using a combination of SuperScript III (Life Technologies), DNA Polymerase I (Enzymatics) and RNAse H (Enzymatics). The resulting cDNA/DNA underwent end repair (End-Repair Mix, Enzymatics), adenylation (Klenow Exo-, Enzymatics; Taq Polymerase, Life Technologies), and ligation (T4 DNA Ligase, Enzymatics) with a universal Y adaptor containing a sample barcode, universal priming site, and Illumina sequencing priming site. Ligated libraries were subjected to two rounds of nested PCR at 10 to 14 cycles each for target enrichment (Platinum Taq Polymerase, Life Technologies). The first round of PCR was performed using a primer complementary to the universal adapter and a first pool of target-specific primers (Operon). A second round of PCR is executed using a 3′ nested universal adapter primer downstream of the first adapter primer and a second pool of 3′ nested target-specific primers downstream of the respective initial first-pool target primers. These nested primers are each 5′ tagged with a common sequencing adapter which, in combination with the first half-functional universal adapter, creates target amplicons ready for clonal amplification and sequencing. Libraries are quantitated using quantitative PCR (Kapa Biosystems), normalized, and processed for sequencing on an Illumina Nextseq 500 instrument according to the manufacturers' standard protocol. Sequencing reads were demultiplexed using Illumina's bcl2fastq script. BWA-MEM was used to align reads to their respective positions according to the NCBI reference genome hg19. Marking of duplicate reads and base quality recalibration is performed using Picard tools and GATK. Suspect chimeric fusion reads after alignment are then called and annotated with a custom script as described (12). For the cohort an average coverage of 200× was obtained per sample, and fusions were prioritized by filtering out known recurrent sequencing artifacts, identifying at least 5 supporting reads, and confirming in-frame status of predicted fusion transcript translated products. The gene and exon targets for fusion analysis are listed in Supplementary Table S1. Site-specific somatic genotyping was performed as described (15), using an adaptation of the Applied Biosystems (ABI) Prism SNaPshot Multiplex system originally developed to detect single nucleotide polymorphisms (SNP). In essence, multiplex PCR with gene-specific primers was followed by primer extension with differentially fluorescent-labeled nucleotides, then extension products were resolved by an

Downloaded from cancerdiscovery.aacrjournals.org on March 27, 2021. © 2017 American Association for Cancer Research.

Published OnlineFirst December 14, 2017; DOI: 10.1158/2159-8290.CD-17-0535

automatic capillary sequencer (ABI PRISM 3730 DNA Analyser, Life Technologies/Applied Biosystems) as described (15). Data analysis for SNaPshot genotyping was performed with GeneMapper Analysis Software version 4.0 (Life Technologies/Applied Biosystems). The gene and residue targets for fusion analysis are listed in Supplementary Table S4.

FISH Analysis

Gene rearrangements were analyzed using a break-apart probe strategy, with two probes spanning the 3′ (spectrum orange label) and 5′ (spectrum green label) ends. In this approach, a fused signal is observed in normal cases, and split signals, green and orange, are seen when translocation is present. BAC clone (probe) searches were performed using the University of California Santa Cruz (UCSC) Genome Browser (http://genome.ucsc.edu/) mapped to December 2013 (GRCh38/hg38) Human Genome Assemblies. BACs were purchased from Children's Hospital Oakland Research Institute (CHORI, Oakland, CA; http://bacpac.chori.org/). BAC clones that showed nonspecific hybridization were discarded. All BAC clones used are shown in Supplementary Fig. S1C. Purified BAC DNA was amplified and directly labeled with spectrum orange or spectrum green dUTPs (Enzo Life Sciences) by nick translation (Abbott Molecular Inc.) according to the manufacturer's protocol. Tissue sections (5 μm) were deparaffinized, pretreated with Tris/EDTA, pH 7.0, and treated with Digest-all (Thermo Fisher) at 37°C for 90 minutes. After washing with 2 × saline sodium citrate (SSC), sections were dehydrated in ethanol and dried. Slides were co-denatured with FISH probes using a Hybrite slide processor (Abbott Molecular Inc.) at 85°C for 5 minutes. Hybridization was performed overnight at 40°C. After hybridization completion, slides were washed two times in 2 × SSC/0.1% Nonidet-40 for 3 minutes each at 72°C, rinsed in water and mounted in Vectashield (Vector Laboratories) containing 4,6-diamino-2-phenylindole (DAPI) as a counterstain. The probes were visualized using an Olympus BX61 microscope and analyzed with Cytovision software (Leica Biosystems). One hundred nuclei were scored in each TMA core, and the positive cases were subsequently confirmed in their tissue blocks. In the tissue blocks, tumor area was located before analysis. The number of "break-apart" or split signals was searched, and a separation of at least two signal diameters was considered as the threshold for a positive split signal. The presence of 5% or more of split signals was indicative of true positive result.

Cell Lines, Cell Culture, and Drug-Sensitivity Studies

Cells were maintained at 37°C in 5% CO_2. MCF7 (ATCC) and T47D (ATCC) cells were grown in RPMI (Lonza) supplemented with 10% FBS (SAFC), 1% penicillin (Gibco), streptomycin (Gibco), and glutamine (Gibco). MCF10A cells were grown in DMEMF12 (Lonza), 5% horse serum (Gibco), 20 ng/mL EGF (Sigma), 10 μg/mL insulin (Sigma), 1 ng/mL cholera toxin (Sigma), and 100 μg/mL hydrocortisone (Sigma). All cell lines except $MCF7^{PIK3CAWT}$ were obtained from the MGH Center for Molecular Therapeutics cell bank in 2016 and 2017 and underwent high-density SNP typing to confirm their identity. For $MCF7^{PIK3CAWT}$ we verified the genotype and cell line identity by a specific PCR assay at the time of receipt (2017) as described (28). All experiments shown were performed within less than 6 months' passage of all lines since acquisition.

To study the fusion-driven effects on canonical E2 targets gene expression, MCF7 cells were cultured in phenol red-free medium with charcoal–dextran-stripped fetal bovine serum for 72 hours, and stimulated with 100 pmol/L of 17β-estradiol (Sigma) for 12 hours.

For 4-OH tamoxifen (selleckchem) and fulvestrant (selleckchem) sensitivity studies, cells were maintained in phenol red-free medium with charcoal–dextran-stripped fetal bovine serum for 48 hours, and 1,000 cells per well were seeded in 96-well plates and exposed to varying doses of 4-OH tamoxifen (10 pmol/L to 1 μmol/L) and fulvestrant (1 nmol/L to 1 μmol/L). Cell proliferation was assayed after 4 days for fulvestrant and 6 days for 4-OH tamoxifen. For MK-2206 (selleckchem) and trametinib (selleckchem) sensitivity studies, cells were cultured in DMEM with 10% FBS, and 1,000 cells were seeded in 96-well plates and exposed to varying doses of MK2206 (1 nmol/L to 1 μmol/L) and trametinib (100 pmol/L to 100 nmol/L) and assayed after 3 days. To determine cell proliferation upon drug treatment, CellTiter-Glo Luminescent Cell Viability Assay (Promega) was used according to the manufacturer's recommendations.

In Vitro Overexpression of Kinase Fusions and RNA Analysis

The cDNA fragments for *CTNNBL1-RAF1*, *ACTL6A-PIK3CA*, and *RPS6KC1-AKT3* were amplified from pDONR223-RAF1, pDONR223-AKT3, and pDONR223-RPS6KC1 (Addgene; ref. 40) and pCIG PIK3CA wild-type (Addgene; ref. 41), respectively. CTNNBL1 was amplified from T47D cells, and an oligonucleotide was designed for ACTL6A (primers and oligos listed in Supplementary Table S7). Constructs were generated by using pENTR Direction TOPO cloning kit (Invitrogen). To generate lentiviral constructs, pLenti CMV Puro DEST (w118-1; Addgene; ref. 42) was used. After verifying by sequencing, pLenti-based kinase fusions were cotransfected into HEK293T cells with lentiviral packaging plasmids pMD2.G and psPAX2 (Addgene) by using the CalPhos Mammalian Transfection Kit (Clontech Laboratories) according to the manufacturer's instruction. The conditioned media containing lentiviral particles were collected 36 hours after transfection and filtered using 0.45-μm pore filter (Millipore). The filtered media were then used to infect target cells. Polybrene (Sigma) was added into filtered media at a final concentration of 10 μg/mL to increase the infection efficiency. The infected cells were selected with 1 μg/μL puromycin (Sigma) 72 hours after infection. Expression of fusion constructs was confirmed via Western blotting.

Total RNA was isolated as described previously (43), and qPCR primers are listed in Supplementary Table S7.

Protein Extraction and Western Blot Analysis

For total protein extraction, cells were lysed in RIPA buffer [10 mmol/L Tris–HCl pH 7.5, 150 mmol/L NaCl, 1 mmol/L EDTA, 1% (w/v) sodium deoxycholate, 0.1% (w/v) SDS, 1% (v/v) NP40, proteinase inhibitor cocktail, phosphatase inhibitor cocktail] for 30 minutes at 4°C.

The protein samples were mixed with SDS sample buffer and boiled for 10 minutes before being subject to SDS-PAGE. The protein samples on the SDS-PAGE gel were then transferred onto PVDF membrane (Milipore), which was blocked by 5% nonfat milk in PBST (PBS plus 0.02% Tween 20) at room temperature for 1 hour. Then, the PVDF membrane was incubated with primary antibodies diluted in 3% BSA in PBST at 4°C overnight and horseradish peroxidase-conjugated secondary antibodies (Sigma) diluted in 3% BSA in PBST at room temperature for 2 hours. The signal was detected by enhanced chemiluminescence solution (PerkinElmer).

Antibodies used are listed in Supplementary Table S8.

3-D Culture, Indirect Immunofluorescence Staining of MCF10A Acini, and Ethidium Bromide Staining Analysis of Cell Death

Three-dimensional culture of MCF10A was performed as described previously (44). Briefly, fusion-expressing MCF10A cells were diluted to a final concentration of 25,000 cells/mL, and Matrigel (Corning) was added in a 1:1 ratio. Matrigel–cell mixture was plated in 8-well chamber slides (lab-tek), 400 μL in each well. Cells were grown in a 5% CO_2 humidified incubator. MCF10A acini cultured in Matrigel were fixed by using an immunofluorescence application solution kit (Cell Signaling Technology) according to the manufacturer's

Downloaded from cancerdiscovery.aacrjournals.org on March 27, 2021. © 2017 American Association for Cancer Research.

Published OnlineFirst December 14, 2017; DOI: 10.1158/2159-8290.CD-17-0535

recommendations. To stain cell–cell junctions, acini were stained with anti–β-catenin (Supplementary Table S8) at 1:100 dilution and secondary Alexa Fluor 488 at 1:200 dilution. To distinguish nuclei, Hoechst 33342 (molecular probes) was used. Prolong Antifade Reagent (Molecular Probes) was used to preserve the slides. Confocal microscopy (Zeiss LSM510 confocal microscope LSM510) was performed as described in Debnath and colleagues (44) with pinhole size of 0.7 to 0.9 μm. Imaris software (bitplane) was utilized for quantification, and at least 200 acini were analyzed per construct. For analysis of cell death during 3-D culture, ethidium bromide (Sigma) was used. After 8 days, 3-D cultures were incubated for 15 minutes with 1 μmol/L ethidium bromide (Sigma) in PBS. Ethidium bromide–positive cells were detected immediately after incubation on the rhodamine channel. Two hundred structures per construct were counted for quantification (20).

Animal Studies

All animals were housed and treated in accordance with protocols approved by the Subcommittee on Research Animal Care at the Massachusetts General Hospital. Female athymic *nu/nu* mice (5–6 weeks) were anesthetized with Avertin (2.5% 2,2,2 tribromoethanol in sterile 1 × PBS) at 16 μL/g (45). Animals were implanted with 60-day slow-release pellets containing 0.72 mg of 17β-estradiol (Innovative Research of America; ref. 46). Xenograft tumors were generated by subcutaneous injections of 8×10^6 T47D cells expressing RPS6KC1-AKT3 or empty vector suspended in 1:1 Matrigel into the mammary fat pad of nude mice. Tumors were measured twice weekly by caliper, and volumes were calculated by the formula $0.5(\text{length}) \times (\text{width})^2$. To mimic tumor growth under E2 deprivation conditions, 17b-estradiol pellets were removed. Palbociclib (LC Labs) was given daily by oral gavage at 150 mg/kg/day for 7 days. Tumor growth was monitored as indicated twice per week or every 2 days (for palbociclib) and tumor volume was measured using the formula $\frac{1}{2}(\text{length} \times \text{width}^2)$.

Statistical Methods

We evaluated the effect of fusions and somatic mutations on three clinical outcomes: overall survival, time from initial diagnosis to metastasis, and survival from time of metastasis. The analyses included data from 101 patients in the Clinical Genotyping Cohort (9 of 110 patients tested were excluded due to missing date of primary diagnosis) and 80 in the Matched Primary/Metastasis Cohort (1 of 81 excluded due to missing data), including 21 who had metastatic disease at the time of initial diagnosis. All patients underwent both AMP and SNaPshot genotyping analysis with the exception of 5 patients lacking SNaPshot data in the Clinical Genotyping Cohort, and 13 lacking SNaPshot data and 18 lacking AMP data in the Matched Primary/Metastasis Cohort. Overall survival was defined as the time from initial diagnosis to death (event) or last follow-up (censored), and the analysis of overall survival included patients with metastatic disease at the initial diagnosis. The analysis of time from initial diagnosis to metastasis excluded patients who were metastatic at initial diagnosis, and event times were observed for all included patients (no censoring). The analysis of time from metastasis to death included both patients who were and were not metastatic at diagnosis. Patients with inadequate data to define a given event time were excluded from the analysis of that event, and those without data for fusion (or mutation) status were excluded from the analyses of the effect of fusion (or mutation) status on each clinical outcome. For the analyses of overall survival and survival from time of metastasis, patients who were known to be deceased but had unknown death dates were treated as alive/censored at the date of last follow-up. Kaplan–Meier curves were constructed to illustrate the relationship between fusions and mutations and each clinical outcome. Cox proportional hazards models were used to assess the association between clinical outcomes and fusions and mutations. These models included the study cohort as a stratification factor which allows for a different underlying hazard function for the two cohorts. Hazard ratios estimated from these models reflect the increase in the hazard rate for a given event associated with positive status for fusion or mutation, with an associated two-sided P value of less than 0.05 indicating a statistically significant association. All other experimental results were analyzed using unpaired two-tailed Student t test or ANOVA, as indicated in figure legends. Groups that were statistically compared shared a similar variance, as shown in the figures. $P < 0.05$ was considered statistically significant.

Disclosure of Potential Conflicts of Interest

Z. Zheng is the inventor of the patented AMP method and is an ArcherDX equity holder. D.M. Finkelstein is a consultant/advisory board member for Gilead and Janssen. L.P. Le has ownership interest (including patents) in ArcherDx and is a consultant/advisory board member for the same. A.J. Iafrate has ownership interest (including patents) in ArcherDx and is a consultant/advisory board member for Roche and Chugai. No potential conflicts of interest were disclosed by the other authors.

Authors' Contributions

Conception and design: K.J. Matissek, M.L. Onozato, S. Sun, Z. Zheng, A. Schultz, K. Patel, S.V. Saladi, M. Debiasi, G. Werutsky, A. Bardia, P.E. Goss, D.C. Sgroi, A.J. Iafrate, L.W. Ellisen
Development of methodology: K.J. Matissek, M.L. Onozato, S. Sun, Z. Zheng, A. Schultz, G. Werutsky, L.P. Le, A.J. Iafrate
Acquisition of data (provided animals, acquired and managed patients, provided facilities, etc.): K.J. Matissek, M.L. Onozato, S. Sun, Z. Zheng, K. Patel, P.-L. Jerevall, S.V. Saladi, M. Tavallai, T. Badovinac-Crnjevic, C. Barrios, N. Beşe, A. Chan, Y. Chavarri-Guerra, E. Demirdögen, H. Gomez, P. Liedke, G. Werutsky, A. Bardia, P.E. Goss, D.C. Sgroi, A.J. Iafrate
Analysis and interpretation of data (e.g., statistical analysis, biostatistics, computational analysis): K.J. Matissek, M.L. Onozato, S. Sun, Z. Zheng, A. Schultz, J. Lee, K. Patel, P.-L. Jerevall, S.V. Saladi, A. Macleay, M. Tavallai, A. Chan, N. Horick, D.M. Finkelstein, L.P. Le, A. Bardia, D.C. Sgroi, A.J. Iafrate, L.W. Ellisen
Writing, review, and/or revision of the manuscript: K.J. Matissek, M.L. Onozato, Z. Zheng, P.-L. Jerevall, T. Badovinac-Crnjevic, C. Barrios, A. Chan, Y. Chavarri-Guerra, M. Debiasi, Ü. Egeli, H. Gomez, P. Liedke, G. Werutsky, J. St. Louis, N. Horick, A. Bardia, P.E. Goss, D.C. Sgroi, A.J. Iafrate, L.W. Ellisen
Administrative, technical, or material support (i.e., reporting or organizing data, constructing databases): K.J. Matissek, A. Schultz, J. Lee, A. Chan, Ü. Egeli, S. Gökgöz, I. Tasdelen, S. Tolunay, J. St. Louis, P.E. Goss, A.J. Iafrate
Study supervision: G. Werutsky, L.W. Ellisen
Other (provided all clinical data and the majority of the biobank): P.E. Goss

Acknowledgments

This work was supported in part by the Avon Foundation Breast Cancer Crusade and the Tracey Davis Memorial Fund. We gratefully acknowledge international collaborators who provided matched primary/metastatic breast cancer specimens, from the Latin America Cooperative Oncology Group (LACOG) including Laura Voelcker, Carlos Sampaio (Pontificia Universidade Catolica do Rio Grande do Sul), Giuliano Borges (Clinica de Neoplasias Litoral), Gustavo Ismael (Fundaçao Amaral Carvalho), Yeni Neron (CEPON), Gabriel Prolla (Hospital Mae de Deus), and Susanne Crocamo (INCA). We also thank Josh Lauring (Johns Hopkins University) for the generous gift of $MCF7^{PIK3CAWT}$ cells.

Downloaded from cancerdiscovery.aacrjournals.org on March 27, 2021. © 2017 American Association for Cancer Research.

Published OnlineFirst December 14, 2017; DOI: 10.1158/2159-8290.CD-17-0535

The costs of publication of this article were defrayed in part by the payment of page charges. This article must therefore be hereby marked *advertisement* in accordance with 18 U.S.C. Section 1734 solely to indicate this fact.

Received May 13, 2017; revised November 9, 2017; accepted December 11, 2017; published OnlineFirst December 14, 2017.

REFERENCES

1. Brisken C. Progesterone signalling in breast cancer: a neglected hormone coming into the limelight. Nat Rev Cancer 2013;13:385–96.
2. Coates AS, Winer EP, Goldhirsch A, Gelber RD, Gnant M, Piccart-Gebhart M, et al. Tailoring therapies–improving the management of early breast cancer: St Gallen international expert consensus on the primary therapy of early breast cancer 2015. Ann Oncol 2015;26:1533–46.
3. Cancer Genome Atlas N. Comprehensive molecular portraits of human breast tumours. Nature 2012;490:61–70.
4. Robinson DR, Wu YM, Vats P, Su F, Lonigro RJ, Cao X, et al. Activating ESR1 mutations in hormone-resistant metastatic breast cancer. Nat Genet 2013;45:1446–51.
5. Toy W, Shen Y, Won H, Green B, Sakr RA, Will M, et al. ESR1 ligand-binding domain mutations in hormone-resistant breast cancer. Nat Genet 2013;45:1439–45.
6. Nik-Zainal S, Davies H, Staaf J, Ramakrishna M, Glodzik D, Zou X, et al. Landscape of somatic mutations in 560 breast cancer whole-genome sequences. Nature 2016;534:47–54.
7. Banerji S, Cibulskis K, Rangel-Escareno C, Brown KK, Carter SL, Frederick AM, et al. Sequence analysis of mutations and translocations across breast cancer subtypes. Nature 2012;486:405–9.
8. Edgren H, Murumagi A, Kangaspeska S, Nicorici D, Hongisto V, Kleivi K, et al. Identification of fusion genes in breast cancer by paired-end RNA-sequencing. Genome Biol 2011;12:R6.
9. Kim J, Kim S, Ko S, In YH, Moon HG, Ahn SK, et al. Recurrent fusion transcripts detected by whole-transcriptome sequencing of 120 primary breast cancer samples. Genes Chromosomes Cancer 2015;54:681–91.
10. Ma Y, Ambannavar R, Stephans J, Jeong J, Dei Rossi A, Liu ML, et al. Fusion transcript discovery in formalin-fixed paraffin-embedded human breast cancer tissues reveals a link to tumor progression. PLoS One 2014;9:e94202.
11. Stransky N, Cerami E, Schalm S, Kim JL, Lengauer C. The landscape of kinase fusions in cancer. Nat Commun 2014;5:4846.
12. Zheng Z, Liebers M, Zhelyazkova B, Cao Y, Panditi D, Lynch KD, et al. Anchored multiplex PCR for targeted next-generation sequencing. Nat Med 2014;20:1479–84.
13. Veeraraghavan J, Tan Y, Cao XX, Kim JA, Wang X, Chamness GC, et al. Recurrent ESR1-CCDC170 rearrangements in an aggressive subset of oestrogen receptor-positive breast cancers. Nat Commun 2014;5:4577.
14. Jang JS, Lee A, Li J, Liyanage H, Yang Y, Guo L, et al. Common oncogene mutations and novel SND1-BRAF transcript fusion in lung adenocarcinoma from never smokers. Sci Rep 2015;5:9755.
15. Dias-Santagata D, Akhavanfard S, David SS, Vernovsky K, Kuhlmann G, Boisvert SL, et al. Rapid targeted mutational analysis of human tumours: a clinical platform to guide personalized cancer medicine. EMBO Mol Med 2010;2:146–58.
16. Gonzalez-Angulo AM, Ferrer-Lozano J, Stemke-Hale K, Sahin A, Liu S, Barrera JA, et al. PI3K pathway mutations and PTEN levels in primary and metastatic breast cancer. Mol Cancer Ther 2011;10:1093–101.
17. Kwak EL, Bang YJ, Camidge DR, Shaw AT, Solomon B, Maki RG, et al. Anaplastic lymphoma kinase inhibition in non-small-cell lung cancer. N Engl J Med 2010;363:1693–703.
18. Muthuswamy SK, Li D, Lelievre S, Bissell MJ, Brugge JS. ErbB2, but not ErbB1, reinitiates proliferation and induces luminal repopulation in epithelial acini. Nat Cell Biol 2001;3:785–92.
19. Shaw KR, Wrobel CN, Brugge JS. Use of three-dimensional basement membrane cultures to model oncogene-induced changes in mammary epithelial morphogenesis. J Mammary Gland Biol Neoplasia 2004;9:297–310.
20. Debnath J, Mills KR, Collins NL, Reginato MJ, Muthuswamy SK, Brugge JS. The role of apoptosis in creating and maintaining luminal space within normal and oncogene-expressing mammary acini. Cell 2002;111:29–40.
21. Ellson CD, Andrews S, Stephens LR, Hawkins PT. The PX domain: a new phosphoinositide-binding module. J Cell Sci 2002;115:1099–105.
22. Turner KM, Sun Y, Ji P, Granberg KJ, Bernard B, Hu L, et al. Genomically amplified Akt3 activates DNA repair pathway and promotes glioma progression. Proc Nat Acad Sci U S A 2015;112:3421–6.
23. Debnath J, Walker SJ, Brugge JS. Akt activation disrupts mammary acinar architecture and enhances proliferation in an mTOR-dependent manner. J Cell Biol 2003;163:315–26.
24. Musgrove EA, Sutherland RL. Biological determinants of endocrine resistance in breast cancer. Nat Rev Cancer 2009;9:631–43.
25. Patani N, Martin LA. Understanding response and resistance to oestrogen deprivation in ER-positive breast cancer. Mol Cell Endocrinol 2014;382:683–94.
26. Lindsley CW. The Akt/PKB family of protein kinases: a review of small molecule inhibitors and progress towards target validation: a 2009 update. Curr Topics Med Chem 2010;10:458–77.
27. Wu P, Clausen MH, Nielsen TE. Allosteric small-molecule kinase inhibitors. Pharmacol Ther 2015;156:59–68.
28. Beaver JA, Gustin JP, Yi KH, Rajpurohit A, Thomas M, Gilbert SF, et al. PIK3CA and AKT1 mutations have distinct effects on sensitivity to targeted pathway inhibitors in an isogenic luminal breast cancer model system. Clin Cancer Res 2013;19:5413–22.
29. Carpten JD, Faber AL, Horn C, Donoho GP, Briggs SL, Robbins CM, et al. A transforming mutation in the pleckstrin homology domain of AKT1 in cancer. Nature 2007;448:439–44.
30. Diehl JA, Cheng M, Roussel MF, Sherr CJ. Glycogen synthase kinase-3beta regulates cyclin D1 proteolysis and subcellular localization. Genes Develop 1998;12:3499–511.
31. Sabnis G, Brodie A. Adaptive changes results in activation of alternate signaling pathways and resistance to aromatase inhibitor resistance. Mol Cell Endocrinol 2011;340:142–7.
32. Sartorius Carol A. ST, Horwitz Kathryn B. Progesterone receptors A and B differentially affect the growth of estrogen-dependent human breast tumor xenografts. Breast Cancer Research and Treatment 2003;79:287–99.
33. O'Leary B, Finn RS, Turner NC. Treating cancer with selective CDK4/6 inhibitors. Nat Rev Clin Oncol 2016;13:417–30.
34. Brown JR, DiGiovanna MP, Killelea B, Lannin DR, Rimm DL. Quantitative assessment Ki-67 score for prediction of response to neoadjuvant chemotherapy in breast cancer. Laboratory Invest 2014;94:98–106.
35. Hart CD, Migliaccio I, Malorni L, Guarducci C, Biganzoli L, Di Leo A. Challenges in the management of advanced, ER-positive, HER2-negative breast cancer. Nat Rev Clin Oncol 2015;12:541–52.
36. Kalinsky K, Jacks LM, Heguy A, Patil S, Drobnjak M, Bhanot UK, et al. PIK3CA mutation associates with improved outcome in breast cancer. Clin Cancer Res 2009;15:5049–59.
37. Davare MA, Tognon CE. Detecting and targetting oncogenic fusion proteins in the genomic era. Biol Cell 2015;107:111–29.
38. Johnston SR. Enhancing endocrine therapy for hormone receptor-positive advanced breast cancer: cotargeting signaling pathways. J Nat Cancer Inst 2015;107.
39. Shah AN, Cristofanilli M. The Growing Role of CDK4/6 Inhibitors in treating hormone receptor-positive advanced breast cancer. Curr Treat Options Oncol 2017;18:6.
40. Johannessen CM, Boehm JS, Kim SY, Thomas SR, Wardwell L, Johnson LA, et al. COT drives resistance to RAF inhibition through MAP kinase pathway reactivation. Nature 2010;468:968–72.
41. Baek ST, Copeland B, Yun EJ, Kwon SK, Guemez-Gamboa A, Schaffer AE, et al. An AKT3-FOXG1-reelin network underlies defective

Downloaded from cancerdiscovery.aacrjournals.org on March 27, 2021. © 2017 American Association for Cancer Research.

Published OnlineFirst December 14, 2017; DOI: 10.1158/2159-8290.CD-17-0535

migration in human focal malformations of cortical development. Nat Med 2015;21:1445–54.
42. Campeau E, Ruhl VE, Rodier F, Smith CL, Rahmberg BL, Fuss JO, et al. A versatile viral system for expression and depletion of proteins in mammalian cells. PloS One 2009;4:e6529.
43. Saladi SV, Ross K, Karaayvaz M, Tata PR, Mou H, Rajagopal J, et al. ACTL6A is co-amplified with p63 in squamous cell carcinoma to drive YAP activation, regenerative proliferation, and poor prognosis. Cancer Cell 2017;31:35–49.
44. Debnath J, Muthuswamy SK, Brugge JS. Morphogenesis and oncogenesis of MCF-10A mammary epithelial acini grown in three-dimensional basement membrane cultures. Methods 2003;30:256–68.
45. Sartorius CA, Shen T, Horwitz KB. Progesterone receptors A and B differentially affect the growth of estrogen-dependent human breast tumor xenografts. Breast Cancer Res Treat 2003;79:287–99.
46. Mohammed H, Russell IA, Stark R, Rueda OM, Hickey TE, Tarulli GA, et al. Progesterone receptor modulates ERalpha action in breast cancer. Nature 2015;523:313–7.

Downloaded from cancerdiscovery.aacrjournals.org on March 27, 2021. © 2017 American Association for Cancer Research.

Published OnlineFirst December 14, 2017; DOI: 10.1158/2159-8290.CD-17-0535

AACR American Association for Cancer Research

CANCER DISCOVERY

Expressed Gene Fusions as Frequent Drivers of Poor Outcomes in Hormone Receptor–Positive Breast Cancer

Karina J. Matissek, Maristela L. Onozato, Sheng Sun, et al.

Cancer Discov Published OnlineFirst December 14, 2017.

Updated version	Access the most recent version of this article at: doi:10.1158/2159-8290.CD-17-0535
Supplementary Material	Access the most recent supplemental material at: http://cancerdiscovery.aacrjournals.org/content/suppl/2017/12/14/2159-8290.CD-17-0535.DC1

E-mail alerts	Sign up to receive free email-alerts related to this article or journal.
Reprints and Subscriptions	To order reprints of this article or to subscribe to the journal, contact the AACR Publications Department at pubs@aacr.org.
Permissions	To request permission to re-use all or part of this article, use this link http://cancerdiscovery.aacrjournals.org/content/early/2018/02/13/2159-8290.CD-17-0535. Click on "Request Permissions" which will take you to the Copyright Clearance Center's (CCC) Rightslink site.

Downloaded from cancerdiscovery.aacrjournals.org on March 27, 2021. © 2017 American Association for Cancer Research.